Slippery Bottom Boundary Layers on a Slope

PARKER MACCREADY * AND PETER B. RHINES

School of Oceanography, University of Washington, Seattle, Washington

(Manuscript received 15 April 1991, in final form 9 December 1991)

ABSTRACT

The turbulent bottom boundary layer for rotating, stratified flow along a slope is explored through theory and numerical simulation. The model flow begins with a uniform current along constant-depth contours and with flat isopycnals intersecting the slope. The boundary layer is then allowed to evolve in time and in distance from the boundary. Ekman transport up or down the slope advects the initial density gradient, eventually giving rise to substantial buoyancy forces. The rearranged density structure opposes the cross-slope flow, causing the transport to decay exponentially from its initial value (given by Ekman theory) to near zero, over a time scale proportional to $f/(N\alpha)^2$, where f is the Coriolis frequency, N is the buoyancy frequency, and α is the slope angle. The boundary stress slowing the along-slope flow decreases simultaneously, leading to a very "slippery" bottom boundary compared with that predicted by Ekman theory.

1. Introduction

When a current flows along constant-depth contours, as is typical of deep boundary currents, the Ekman transport in the bottom boundary layer will tend to move water up or down the slope. If there is a density gradient across the slope, this displacement gives rise to a buoyancy force, which eventually becomes comparable with the other terms in the Ekman balance. The shifted density field causes a vertical shear in the initial current (via the thermal wind) slowing it near the boundary, and leaving less to be done by viscous stress. Rhines and MacCready (1989), MacCready and Rhines (1991), Trowbridge and Lentz (1991), and MacCready (1991) find that both the boundary stress and the Ekman transport decrease over time as a result, leading to a boundary-layer solution markedly different from the standard Ekman layer. This process will be referred to as the "shutdown" of the boundary layer.

The spindown of ocean circulation (e.g., Holton 1965; Walin 1969), resulting from vortex stretching driven by Ekman pumping, is a cornerstone for our ideas of ocean dynamics. The decreased Ekman transport suggested in the previous papers causes major modifications to the spindown process, leading to a nearly frictionless lower boundary condition for some deep flows. In the following, we derive an expression (with numerical support) for the time scale over which a model turbulent boundary layer on a slope will shut down to help judge whether the proposed buoyancy effects may be important to a given flow.

Several authors in the last 25 years have explored the general idea of a boundary layer on a slope with stratification and rotation, although it is only recently that the phenomenon of decreased Ekman transport has been recognized. Past theoretical discussions, like this work, mainly involved one-dimensional models, with variation only in distance from the slope, and occasionally also in time, invoking the usual approximation that the boundary layer is thin compared with horizontal variation in the flow parameters [a notable exception is the two-dimensional model of Ezer and Weatherly (1990) of the "cold filament" in the North Atlantic]. The earliest solutions to the one-dimensional problem, arrived at independently by Holton (1967) and Hsueh (1969), are essentially steady, differing little from the classic Ekman solution. These authors specify the density at the boundary, as may be appropriate for atmospheric flows over the ground, with the result that fluid advected up- or downslope tends to adjust to the density of its surroundings, and hence, no large buoyancy force develops. In the ocean, however, the correct condition (in the absence of substantial geothermal heating) is that there be zero density flux at the boundary, that is, an "insulating" boundary.

Weatherly and Martin (1978) and Thorpe (1987) solve the steady problem with zero density flux at the boundary, but the result has a very curious property that limits its applicability in the ocean. Unlike the atmospheric solutions of Holton (1967) and Hsueh (1969), the steady, insulating solution requires that the interior, along-slope flow possess a specific value

* Current affiliation: Rosenstiel School of Marine and Atmospheric Sciences, University of Miami.

Corresponding author address: Dr. Parker MacCready, RSMAS/MPO, 4600 Rickenbacker Causeway, Miami, FL 33149-1098.

related to the slope angle, stratification, diffusivity, etc. That is, the interior velocity *is a part of the solution.* In addition, the steady theory demands that the value of the cross-slope transport be κ_∞/α, where κ_∞ is the eddy diffusivity of density in the interior, and α is the angle of the slope from horizontal (assumed small). The reason for this constraint on the transport is that the steady solution must satisfy a global balance between diffusive flux of density upwards in the interior and advection of density upslope within the boundary layer. It is clear that this result must not describe the boundary layer over flat regions, where it predicts infinite transports. For constant coefficients of diffusivity there is only one along-slope flow that will yield the required transport.

There is, of course, a serious question confronting a boundary-layer theory that sets its own interior velocity: Does the interior flow control near-boundary adjustment or vice versa? To address this, Thorpe solves the steady problem with a fixed eddy diffusivity profile that varies in distance from the boundary (high next to the boundary and low in the interior). He finds that by making different choices of eddy diffusivities and mixed-layer thickness one may arrive at different steady values for the interior along-slope velocity (although the resulting solutions are not always statically stable). Garrett (1990, 1991) takes this idea farther, deriving an expression for the interior velocity for any diffusivity profile and suggesting that the profiles could "self adjust" such that the given interior flow would be the correct one to match the steady solution. Once again, though, the constraint of static stability is felt, and Garrett concludes that this adjustment process would likely occur only for flows that initially had downslope Ekman transport. Thus, we are left with some doubt about the general applicability of a steady approach to the problem, although one must certainly not disregard steady solutions, as they are the end states toward which any unforced, time-dependent flow must tend.

For time-dependent flows that include buoyancy and momentum forcing, as in the ocean, the time over which the steady solution is achieved becomes, then, crucially important. If a given steady solution is rapidly achieved by Garrett's self-adjustment process, then one could reasonably look to it for information on bottom stress and boundary mixing of density and other tracers. If, on the other hand, a steady solution is only slowly achieved, then it may be overwhelmed by the forcing, and have little influence on observed flows.

Thus, to understand how these boundary layers apply to the ocean it becomes necessary to explore the time-dependent problem. Thorpe (1987) considers an alongslope flow with oscillatory time dependence, but the average transport of his solution is the same as that of the steady solution and presents many of the same difficulties. Weatherly and Martin (1978), in a ground breaking study, develop unsteady numerical solutions to the problem, using a Mellor and Yamada (1974) turbulence closure scheme to predict eddy diffusivities near the boundary and comparing their results with observations on the edge of the Florida shelf. Their model flow starts from rest, and then an alongslope current is turned on to drive the boundary layer. They observe differences in mixed-layer thickness depending on whether the flow has upslope or downslope transport, and show that cross-slope advection of the density gradient is the cause, although they do not make the connection between buoyancy forces and temporal changes in the Ekman transport or boundary stress.

MacCready and Rhines (1991) explore the sloping boundary-layer problem through theory and numerical simulation, using the same sort of impulsively started current as Weatherly and Martin but with constant diffusivity coefficients in order to compare with laboratory experiments on stratified spinup in a bowl with sloping sidewalls. Early in time the solutions resemble the classic Ekman layer, but later the cross-slope transport and the along-slope stress decay approximately as $(\text{time})^{-1/2}$, owing to the type of buoyancy effects described at the start of this section. An expression is derived for the "shutdown time" for laminar flows, and it is confirmed that Thorpe's steady solution is the final state toward which the flow tends. Recall, however, that the steady solution has a required interior velocity, so one must in general affect the *entire* water column before a steady state is possible. Such an occurrence seems unlikely for a one-dimensional boundary layer in a rotating system, which typically only grows to a very limited Ekman thickness. The reconciliation suggested to this seeming contradiction is that, in the same way that the cross-slope flow is variable in time, the alongslope velocity is also time dependent, obeying a modified diffusion equation, and the value toward which this velocity diffuses (from the bottom) is that of Thorpe's steady solution. Thus, for the laminar, one-dimensional case, one has a fair idea of the time required to reach the steady solution, and of the means by which the alongslope flow may adjust to its required steady value.

Trowbridge and Lentz (1991) have recently extended the analysis of the time-dependent, impulsively started problem to include a mixed layer, in order to make comparisons with data from the Coastal Ocean Dynamics Experiment. They use the slab mixed-layer model of Pollard et al. (1973), and a velocity-squared drag law for the bottom stress. They observe the decay of the Ekman transport with time; however, their model does not allow a simple expression of the shutdown time, and they focus, as did Weatherly and Martin (1978), on the prediction of mixed-layer thickness.

In the present paper we build on the previous work to derive an expression for the shutdown time when there is an evolving, turbulent mixed layer, with both theoretical and numerical support. We also address the diffusivelike changes to the interior along-slope flow and their relation to the steady solution.

2. Governing equations and shutdown scaling estimates

Can boundary-layer dynamics really be affected by the weak stratifications typical of the ocean? Standard scaling arguments (Pedlosky 1987, pp. 360–362) suggest that the oceanic bottom boundary layer may be treated as homogeneous, owing to its thinness and the weakness of the stratification. However, advection of density gradients on a slope will eventually invalidate this scaling.

a. Basic shutdown time estimate

The time it takes for buoyancy to become important may be easily estimated. Consider the near-boundary advection that occurs beneath a uniform current V, along a slope of angle α, with interior buoyancy frequency N (Fig. 1). The fluid near the boundary is slowed by viscosity, and so feels a pressure force upslope (for V negative) that is not in balance with its Coriolis force. The fluid accelerates upslope, but an opposing buoyancy force, $-g\rho'\alpha$, arises over time to oppose that acceleration (assume $\alpha \ll 1$). Here g is gravity, and ρ' is the perturbation to the initial stratification of the fluid, which one may also scale as $\rho' \approx [(\rho_0/g)N^2\alpha] \times [\Delta\hat{x}]$, assuming that the density at a point has changed only owing to advection of the initial stratification ($\Delta\hat{x}$ is the cross-slope displacement of a fluid parcel). Since the cross-isobar velocity in the Ekman layer scales as $-V$, we may say that after a time τ_0 the term $\Delta\hat{x}$ will be about $-\tau_0 V$. The downslope buoyancy force will thus be $\rho_0 N^2\alpha^2(\tau_0 V)$, which will be of the same magnitude as the initial (upslope) Coriolis force, $f\rho_0 V$, by the time:

$$\tau_0 = \frac{f}{(N\alpha)^2}. \tag{2.1}$$

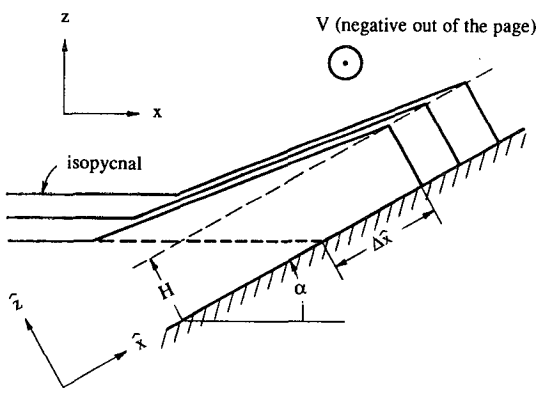

FIG. 1. Slope frame of reference for the coordinate system ($\hat{x}$, $\hat{y}$, $\hat{z}$) in which the equations of motion are developed, along with definitions of mixed-layer thickness H, slope angle α, interior alongslope velocity V, and cross-slope displacement $\Delta\hat{x}$. The isopycnals are shown as they would be displaced by strong mixing near the boundary and by the upslope Ekman transport associated with an interior alongslope velocity of negative sign.

This time, τ_0, derived more formally in MacCready and Rhines (1991), is the simplest estimate of the shutdown time, or the time when buoyancy forces become important to the boundary layer on a slope. In this derivation we have tacitly assumed that the mixed-layer thickness, H, is equal to the Ekman layer thickness, and so diffusive changes to ρ' will be unimportant compared with advective changes. In section 2c we address this problem using a more refined theory.

b. Governing equations

For a more precise idea of the shutdown behavior in the case with a turbulent boundary layer, we must formally develop the equations. Begin with flow along a slope of constant angle, α. If the alongslope flow is initially homogeneous and the fluid Boussinesq, as we assume, the problem is greatly simplified, having then variation only in the direction normal to the slope (and in time). These assumptions, as in the development of the classic Ekman layer, lead to solutions that are locally valid if the space and time scales of variation of the flow parameters are large and slow compared with those of the solutions.

Following Phillips (1970), and using the notation of MacCready and Rhines (1991), the equations of momentum and mass conservation in the boundary layer are

$$\frac{\partial\hat{u}}{\partial t} - f(\hat{v} - V) = -\alpha B + \frac{\partial}{\partial\hat{z}}\left(\nu\frac{\partial\hat{u}}{\partial\hat{z}}\right), \tag{2.2}$$

$$\frac{\partial\hat{v}}{\partial t} + f\hat{u} = \frac{\partial}{\partial\hat{z}}\left(\nu\frac{\partial\hat{v}}{\partial\hat{z}}\right), \tag{2.3}$$

$$\frac{\partial B}{\partial t} = N^2\alpha\hat{u} - N^2\frac{\partial\kappa}{\partial\hat{z}} + \frac{\partial}{\partial\hat{z}}\left(\kappa\frac{\partial B}{\partial\hat{z}}\right). \tag{2.4}$$

Equations (2.2)–(2.4) are for velocities in the "slope frame of reference," that is, rotated by an angle α from the horizontal (we assume throughout that $\alpha \ll 1$, so $\cos\alpha \approx 1$ and $\sin\alpha \approx \alpha$). Variables in this frame of reference are denoted by a caret on top if there is any chance for confusion with variables in the nonrotated frame of reference. As in Fig. 1, upslope is the positive $\hat{x}$ direction, while the normal to the slope is the positive $\hat{z}$ direction (the y direction is unchanged since the coordinate frame was rotated about that axis, and there is no variation in that direction). Similarly, $\hat{u}$ is the upslope velocity, and $\hat{v}$ is the alongslope velocity, where positive $\hat{v}$ is into the page in Fig. 1. Here V is a geostrophic, alongslope velocity related to an imposed pressure gradient in x, switched on to a constant value at $t = 0$ (thus, the pressure does not appear explicitly). B is the (negative of the) buoyancy, given by

$$B \equiv g\rho'/\rho_0. \tag{2.5}$$

We have divided the density into three parts as

$$\rho = \rho_0 + \bar{\rho}(z) + \rho'(\hat{z}, t), \tag{2.6}$$

and $\bar{\rho}$ is defined by the buoyancy frequency, N, where

$$N^2 \equiv \frac{-g}{\rho_0}\frac{\partial \bar{\rho}}{\partial z}, \tag{2.7}$$

which is taken to be constant. We make the Boussinesq approximation: $\bar{\rho} \ll \rho_0$, and $\rho' \ll \rho_0$, but otherwise the flow-induced perturbation ρ' can equal or exceed $\bar{\rho}$ in magnitude, leaving open the possibility of static instability.

We take $\hat{w}$ to be zero everywhere, and parameterize the effects of vertical eddy velocities through coefficients of eddy diffusivity: ν for momentum and κ for density. The coefficients are variable in time and $\hat{z}$, to allow solutions with an evolving mixed layer, as often observed in the ocean.

Equations (2.2) and (2.3) describe a time-dependent Ekman layer, with the important addition of a buoyancy term, $-\alpha B$, on the right-hand side of (2.2). From (2.4) we see that this buoyancy term grows in magnitude owing to advection of the mean stratification, N^2, by the cross-slope velocity, $\hat{u}$, as well as being modified by density diffusion. With κ large near the boundary and small in the interior, the chief effect of the diffusive terms in (2.4) is to cause a mixed layer in the density profile in the region where κ is greater.

At the lower boundary we assume a no-slip condition on the velocity, and no diffusive flux of density out of the boundary. Hence,

$$\hat{u} = \hat{v} = 0 \quad \text{at} \quad \hat{z} = 0, \tag{2.8}$$

and

$$\frac{\partial B}{\partial \hat{z}} = N^2 \quad \text{at} \quad \hat{z} = 0. \tag{2.9}$$

The upper boundary conditions are that

$$\hat{u}, B \to 0 \quad \text{as} \quad \hat{z} \to \infty, \tag{2.10}$$

and

$$\hat{v} \to V \quad \text{as} \quad \hat{z} \to \infty. \tag{2.11}$$

Initially, the $\hat{u}$ and B fields are set to zero, and the alongslope velocity is set to V everywhere (except at the boundary, where it is also zero). The specification of the problem is then complete except for a relation to determine the eddy diffusivities, which is given in section 3 for the numerical integrations.

c. *An approximate theory of shutdown*

We may simplify the problem to form an analytic solution to the time-dependent problem, yielding a much better estimate of the shutdown time, as well as some ideas about the actual velocity and density profiles. First, assume that we have a turbulent mixed layer of height H, which may be time dependent, with momentum eddy diffusivity ν_0 inside and no diffusivity of momentum or density outside. Further, assume that the density within the boundary layer is well mixed normal to the slope, which may be written as

$$\frac{\partial B}{\partial \hat{z}} = N^2 \quad \text{for} \quad 0 \leqslant \hat{z} \leqslant H, \tag{2.12}$$

and that there is no flux of density through the bottom boundary or through the top of the mixed layer. Note that (2.12) satisfies both the upper and lower density boundary conditions. All further calculations in this subsection pertain to the mixed layer $0 \leqslant \hat{z} \leqslant H$; the fields beyond H do not change with time. Using (2.12) the density equation immediately simplifies to

$$\frac{\partial B}{\partial t} = N^2 \alpha \hat{u}, \tag{2.13}$$

which we may integrate over the mixed layer to find

$$\frac{\partial B}{\partial t} = \frac{N^2 \alpha}{H} M, \tag{2.14}$$

where M is the cross-slope transport, defined as

$$M \equiv \int_0^H \hat{u} d\hat{z}. \tag{2.15}$$

Since B has a constant gradient over the mixed layer, its time derivative will be constant in $\hat{z}$ over that region, facilitating the integration to find (2.14). [Mathematically it is helpful to think of the buoyancy term in the boundary layer as a $\hat{z}$ integral of (2.12): $B(\hat{z}, t) = N^2\hat{z} + C(t)$, where C is a constant of integration, variable only in time.]

Although we assumed the density to be well mixed below $H(t)$, we now proceed by making the seemingly contradictory assumption that the velocities are not necessarily well mixed, despite the fact that the diffusivities of momentum and density are likely to be equal in the boundary layer. The boundary conditions on the velocities are very different from those on the density, however. While the no-flux conditions tend to homogenize the density, the no-slip condition may support considerable velocity shear. This idea is also consistent with numerical solutions to (2.2)–(2.4) presented in the following section.

Now to solve the momentum equations we begin by dropping the acceleration terms in (2.2) and (2.3), as suggested by Gill (1981) and Trowbridge and Lentz (1991), on the grounds that they only contribute significantly to inertial oscillations, which are, for oceanic scales, just small perturbations to the fundamental shutdown solution (also, examination of these terms in the following numerical integrations will show that they are negligibly small after about one pendulum day). We may then rewrite the momentum equations in the boundary layer as

$$-f\left[\hat{v} - \left(V + \frac{\alpha B}{f}\right)\right] = \nu_0 \frac{\partial^2 \hat{u}}{\partial \hat{z}^2}, \tag{2.16}$$

and

$$f\hat{u} = \nu_0 \frac{\partial^2 \hat{v}}{\partial \hat{z}^2}, \tag{2.17}$$

with no slip at $\hat{z} = 0$, and no stress at $\hat{z} = H$. This is a steady Ekman layer problem, but with parametric time dependence through the term B, which, as seen in (2.14), changes through the cross-slope transport of the stratification. Equations (2.16)–(2.17) are then solved in the usual way (it is helpful to take $\partial/\partial t$ of both equations first, to eliminate the $\hat{z}$ dependence in B). For simplicity, we present here the solution in the limiting case $H \gg \delta_0$, where δ_0 is the natural Ekman layer scale of the problem, $(2\nu_0/f)^{1/2}$. MacCready (1991) presents the full solution for arbitrary H, and finds that this limit differs little from it, as long as $H \geqslant \delta_0$. We find (after taking a time derivative and integrating in $\hat{z}$ to find the transport) that

$$\frac{\partial B}{\partial t} = \frac{-2f}{\alpha \delta_0} \frac{\partial M}{\partial t}. \tag{2.18}$$

Combining (2.18) with the result from the buoyancy equation (2.14), we may form an equation for the transport:

$$\boxed{\frac{\partial M}{\partial t} = \frac{-1}{D\tau_0} M} \tag{2.19}$$

where

$$D \equiv 2H/\delta_0, \tag{2.20}$$

and $\tau_0 \equiv f/(N\alpha)^2$, as before. Thus, the shutdown time for this problem is $D\tau_0$, proportional to our original estimate (2.1). The shutdown time increases with H because the density gradient advected by the cross-slope flow is distributed by mixing over a thickness H, diluting the effect of buoyancy in the momentum equations. This is the main failing of our initial scaling (2.1), which essentially assumed δ_0 and H to be identical. When H is constant in time, as is typical when M is upslope, (2.19) implies exponential decay of the transport in time from its initial value given by Ekman theory without any buoyancy effects (assuming $D\tau_0 \gg f^{-1}$). When M is downslope, however, H increases in time (Weatherly and Martin 1978; Trowbridge and Lentz 1991) because the advection of lighter water under heavier leads to static instability. In this case (2.19) is not easily solved, but still it implies that *at any given time* the decay time scale of the transport is $D\tau_0$, an idea used in section 3 for comparisons with the numerical solutions.

Since the first observations of the ocean-bottom mixed layer (e.g., Armi and Millard 1976), a classic question has been the relation between the momentum boundary layer and the buoyancy boundary layer. One often reads that the deep mixed layer in temperature and salinity may be much thicker than the turbulent Ekman layer, a possibility that our model allows. While the quantities H and δ_0 may not be exact descriptions of oceanic parameters (owing to the greater complexity of real boundary layers) they should still be useful as a way to "translate" from an observed flow to an expected shutdown time. For example, one could choose the value of δ_0 for a real flow based on the Ekman transport it developed (when the effects of buoyancy were negligible) as opposed to the actual thickness of the boundary layer. The beginnings of such applications are presented in MacCready (1991), for the Costal Ocean Dynamics Experiment, and the Deep Western Boundary Current in the North Atlantic.

MacCready and Rhines (1991) develop approximate solutions to (2.2)–(2.4) with ν and κ constant, and find a shutdown time for that case. Their main strategy is to assume that the along-slope flow is in thermal-wind balance. This proves useful for the laminar case over most of the boundary layer, and they find that the transport decreases as $t^{-1/2}$ (after the initial setup of Ekman-like flow) with the time scale of the decay given by

$$\tau_{\text{laminar}} = \frac{1}{S}\left(\frac{1/\sigma + S}{1 + S}\right)\tau_0, \tag{2.21}$$

where $S \equiv (N\alpha/f)^2$, a Burger number, and $\sigma \equiv \nu/\kappa$. The transport decays towards its final value, κ/α. Note that when $\sigma \gg 1$ (negligible density diffusion), and $S \ll 1$ (e.g., small slope), the shutdown time reduces to our simple estimate, τ_0.

Trowbridge and Lentz (1991) approach the problem with a turbulent boundary layer using a slab mixed-layer model similar to that of Pollard et al. (1973). They average $\hat{u}$, $\hat{v}$, and ρ through the depth of the mixed layer and use a drag coefficient and velocity-squared drag law to determine stress at the boundary. Their mixed-layer height increases if the bulk Richardson number falls below a critical value. Thus, they encompass somewhat realistic mixed-layer height dynamics [which they use to great advantage when making comparisons with ocean data in Lentz and Trowbridge (1991)], although they do not resolve actual velocity profiles in the mixed layer. In addition, they develop equations describing the initial decay of the cross-slope transport. The equations are too complicated to solve in general, except numerically, but still yield insight into the shutdown phenomenon. If we assume that the mixed-layer height maintains a constant thickness (clearly a better approximation in the upwelling case than in the downwelling case) then one may find from their analysis that the transport *initially* decays exponentially in time, similar to the solution (2.19), and the time scale, τ_{TL}, for the decay is (J. Trowbridge, personal communication):

$$\tau_{\text{TL}} = \frac{(1 + \beta)(1 + 2\beta)}{\sqrt{\beta}(2 + \beta)}\tau_0, \tag{2.22}$$

where

$$\beta \equiv \frac{\sqrt{2}}{2}\frac{C_d N}{f}, \tag{2.23}$$

and C_d is the drag coefficient. For $N = 3.5 \times 10^{-3}$ s^{-1}, $f = 10^{-4}$ s^{-1}, and $C_d = 2.5 \times 10^{-3}$ (their value), then $\beta = 0.06$ and $\tau_{TL} = 2.4\ \tau_0$ (the same value we would predict for $H/\delta_0 = 1.2$). Of course their full equations, which include changing mixed-layer heights, would give a somewhat different answer than this. Nevertheless, (2.22) serves as a useful comparison. It is encouraging that both $\tau_{laminar}$ and τ_{TL} are proportional to τ_0, or $f/(N\alpha)^2$, as is our estimate $D\tau_0$, despite the differences in how the flow is modeled. One may thus think of τ_0 as the "base" value of the shutdown time, with variations from that owing to the nature of the diffusivities in the boundary layer.

d. *Other scales of the boundary layer*

Buoyant shutdown of the Ekman flow has the remarkable property that the developing shift of the isopycnal surfaces, caused by the cross-slope transport (and mixing), tends to establish a thermal wind–balanced vertical shear that, of its own accord, brings the velocity to zero at the boundary. In terms of the pressure field, the sign of the buoyancy force is such as to cancel out the cross-slope pressure gradient of the initial, interior, geostrophic velocity. For either positive or negative V, the corresponding downslope or up-slope advection of the density field always tends to relieve the flow of the need for a viscous boundary layer. Stratified spindown also has this property: interior isopycnals are rearranged by Ekman pumping and the resulting thermal wind shear brings the flow to rest at the boundary. But note the differences: spindown requires a curl of the interior flow, while shutdown does not; also spindown may affect flow deep in the interior, beyond the direct reach of viscosity, while shutdown is confined to the thickness of the viscous boundary layer (which may, however, grow rather larger than one expects; see section 4).

For downwelling-favorable flows (where the initial transport is downslope, that is, positive V) Trowbridge and Lentz propose a steady, inviscid solution with linear shear in the alongslope flow. As in MacCready and Rhines (1991), they assume that the current is in thermal wind balance, and then combine that with a density field that is vertically homogeneous in the boundary layer. The maximum shear that the thermal wind may support is $\alpha N^2/f$, and the mixed layer must have a thickness of at least

$$H_{min} = fV/(N^2\alpha), \tag{2.24}$$

in order to bring the alongslope flow to rest at the boundary. Such a solution is evident in the downwelling-favorable numerical solutions presented in the following section, and is implicit in (2.16).

Another useful scale for the shutdown process is the distance up or down the slope, $\Delta\hat{x}$, that isopycnals at the boundary must be displaced to bring the alongslope flow to rest. This is found from our initial scaling of the shutdown time (section 2a) to be

$$\Delta\hat{x} = -fV/(N\alpha)^2, \tag{2.25}$$

which is, of course, the same as $V\tau_0$. One may also derive $\Delta\hat{x}$ from a vertical integral of the thermal wind equation. To the extent that viscous and time-dependent effects are negligible within the shutdown boundary layer, $\Delta\hat{x}$ should be a much more robust estimate than τ_0, which we saw to be greatly modified by H/δ_0. Note that while H_{min} applies only to downwelling-favorable flows, $\Delta\hat{x}$ applies equally to upwelling or downwelling-favorable situations.

Using values typical of the ocean we may use the foregoing scales to estimate when buoyancy forces may be important. Assume in one case that we are on an abyssal plain, with $\alpha = 10^{-3}$, $N = 10^{-3}$ s^{-1}, and $f = 10^{-4}$ s^{-1}. Then H_{min} is 10 km (for $V = 0.1$ m s^{-1}), considerably larger than we imagine the benthic boundary layer to be. The value of $\Delta\hat{x}$ in this situation is 1000 km, also rather large. The basic shutdown time, τ_0, is 3.2 years. These values lead us to conclude that one may probably ignore buoyancy effects on an abyssal plain.

If, however, we make the same calculations on the continental slope, with $\tan\alpha = 10^{-2}$, and $N = 3.5 \times 10^{-3}$ s^{-1}, we find H_{min} is 81.6 m (again for $V = 0.1$ m s^{-1}), and $\Delta\hat{x}$ is about 8 km. The basic shutdown time is just under a day. Clearly, buoyancy may be important for this case.

3. Numerical integrations

The coupled set of momentum and mass conservation equations (2.2)–(2.4) were integrated numerically using central differencing in space and forward differencing in time. This integration scheme has the virtue of simplicity, and works well for the diffusive parts of the equations, but it is well known that forward differencing is unconditionally unstable for inertial oscillations. This shows up as a "wrinkling" at the grid scale, evident in some of the numerical results, but the instability grows very slowly, is damped out by the diffusivity, and does not significantly affect the results over the time of the integrations. Tests of accuracy of the code were carried out, using the known analytic solution (Greenspan 1969, pp. 30–34) to the transient Ekman layer problem with constant diffusion coefficients. The numerical solution arrived at the correct profiles, with transients at the inertial frequency decaying in amplitude as $t^{-1/2}$, as the theory predicts.

The lower boundary conditions used were no slip (2.8) and insulating (2.9). To take gradients numerically at the boundary, where central differencing does not work, we used upward differencing plus a correc-

tion based on the second derivative of the field at the grid point above the slope. The upper boundary of the integration was always sufficiently far away that it did not affect the solution. Initially both $\hat{u}$ and B were zero for all $\hat{z}$, while $\hat{v}$ was set to V for all $\hat{z}$ except at the boundary, where it was set to zero.

In MacCready and Rhines (1991) we used constant coefficients of diffusivity for our numerical simulations, modeling laboratory experiments where the flows were laminar and the diffusivity was molecular. The present model allows variable diffusivities, although the exact way to parameterize that variability is the subject of some debate; different researchers employ everything from Mellor–Yamada level II turbulence-closure schemes (Weatherly and Martin 1978) to "slab" mixed-layer models (Trowbridge and Lentz 1991). Actual ocean data are so sparse that it would be difficult to decide which model was the "best" representation of the actual boundary-layer physics.

We chose to use a model of intermediate complexity, assuming that the diffusivities are a simple function of the gradient Richardson number, Ri, defined here as:

$$\mathrm{Ri} \equiv \frac{-g}{\rho_0}\frac{\partial \rho}{\partial \hat{z}}\left[\left(\frac{\partial \hat{u}}{\partial \hat{z}}\right)^2 + \left(\frac{\partial \hat{v}}{\partial \hat{z}}\right)^2\right]^{-1}. \qquad (3.1)$$

Price et al. (1986) add such a parameterization to the Pollard et al. (1973) slab upper-ocean model, with apparent success. We take the diffusivities to be large, 100 $\mathrm{cm^2\ s^{-1}}$ ($10^{-2}\ \mathrm{m^2\ s^{-1}}$), when Ri is below 0.2, and small, 1 $\mathrm{cm^2\ s^{-1}}$ ($10^{-4}\ \mathrm{m^2\ s^{-1}}$), when Ri is greater than 0.3. We will refer to the larger limit on the diffusivities as ν_0 or κ_0, while the lower limit will be called ν_∞ or κ_∞. Between these two values of Ri the diffusivities decrease linearly with increasing Ri, as shown in Fig. 2. The diffusivities of momentum and density are set equal, since the fluxes are assumed to be due to turbulence. (This need not be so if internal waves are allowed to transport momentum, but then we would expect any diffusion equation to be a poor description of the momentum field redistribution.) Since our numerical model has eddy diffusivities based solely upon Richardson number, and not distance from the boundary, we are unable to model the logarithmic layer that presumably inhabits the lowest meter or so. This omission should change only the details of the velocity profiles but should not significantly alter the dynamics of shutdown, which is our interest here.

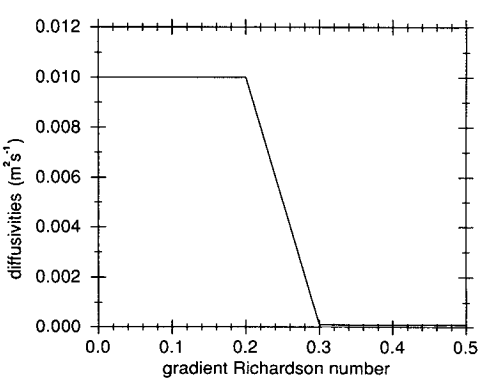

FIG. 2. Plot of eddy diffusivity coefficients versus gradient Richardson number, used in the numerical solution of the equations of motion. The lower limiting value of the diffusivities is $10^{-4}\ \mathrm{m^2\ s^{-1}}$, and the critical Richardson number is around 0.25.

Our diffusivity profile thus assumes a critical Richardson number of about 0.25. The ramp in the diffusivities between $0.2 < \mathrm{Ri} < 0.3$ is motivated by the range of turbulent dissipation rates observed in the benthic boundary layer (e.g., Dewey et al. 1988). The very nature of such a mixing model often gives rise to a mixed layer of nearly constant density capped by a small region of strong density gradients, along with high dissipation in the mixed layer and low dissipation above. This tendency is observed both in the ocean and in the numerical results that follow, but observed fields of dissipation also often have more structure than a simple two-layer model will allow. We leave that possibility open in our numerical model by using a ramp in the diffusivity–Ri curve, instead of a step.

The upper limit for diffusivity is based loosely on direct turbulence measurements taken in the benthic boundary layer and equatorial undercurrent (Trump 1983; Thorpe 1987; Gregg 1987). Placing an upper bound on the diffusivity means that the density profile may become gravitationally unstable, if advection overpowers the diffusivity. Limiting the maximum diffusivity puts a lower bound on the time-step size, however, which is numerically convenient, so we just avoid driving the model with velocities so large as to cause gravitationally unstable profiles. The lower value of diffusivity we use outside the boundary layer is Munk's (1966) value, derived from an advective–diffusive balance in the Pacific. Some have suggested that most of the deep mixing in the oceans occurs at the boundaries, complicating any notion of an interior vertical eddy diffusivity (e.g., Garrett 1990). Our philosophy in the numerical modeling has been simply to assume that there is some vertical diffusivity in the interior that is very much smaller than that in the turbulent mixed layer. For numerical stability it is necessary to have a nonzero diffusivity in the interior, but the actual value of that diffusivity has little effect on the boundary-layer development during the initial shutdown (as long as $\nu_\infty \ll \nu_0$). In the steady solutions, however, the value of the interior diffusivity is crucially important, particularly to the cross-slope transport, which is required to be κ_∞/α, as stated earlier.

Sensitivity studies were carried out using different forms of the diffusivity–Ri curve. In one case, the ramp in the diffusivities was placed between Ri = 0.5 and Ri = 1.5 (essentially a fourfold increase in the critical Richardson number). This gave rise to thicker mixed layers, as one would expect, and the size of the increase was about 50%. Thus, the model was not overly sen-

sitive to the details of the diffusivity–Ri relation, at least for early times. At later times, however, the results may be very sensitive to this choice. Garrett (1991) (and see section 4) derives a steady estimate of the Richardson number in the mixed layer, which one may use to determine the eddy diffusivities there. Depending upon which side of the critical Ri the solution lands, one may end up then with substantially more or less late-time mixing of passive tracers in the boundary layer.

a. Upwelling-favorable case

The six plots of Fig. 3 document different aspects of a three-day numerical integration of (2.2)–(2.4). We initiated the integration with an alongslope flow, V, of -0.1 m s^{-1}. In the absence of buoyancy effects this would give rise to an Ekman layer with upslope transport, so we refer to this case as upwelling favorable. The parameters were the same as those used in the continental slope example in section 2d ($\tau_0 = 0.94$ days). The vertical resolution was 1 m, and the time step 8 s. Figure 4 is from a numerical run using the same parameters as in Fig. 3, but the integration was carried out to 18 days, showing the behavior of the flow after it was fully shut down.

One-half day into the integration, the cross-slope velocity profile (Fig. 3a) had roughly the thickness of an Ekman layer based on ν_0, which is $\delta_0 = (2\nu_0/f)^{1/2}$, or 14 m for our integrations. Later in the integration the cross-slope current decreased in both magnitude and thickness. This decrease was also present in the transport (the vertical integral of the upslope velocity), shown in Figs. 3f and 4f. The oscillations in the transport were inertial waves excited by the abrupt startup of the flow. The natural frequency of these oscillations, predicted by Weatherly and Martin (1978) and confirmed by these runs, is $f(1 + S)^{1/2}$ [recall $S \equiv (N\alpha/f)^2 = 0.12$ in this case]. At first the transport increased rapidly to approximately the value it would have based on steady Ekman theory: $-V\delta_0/2$, which is 0.7 m^2 s^{-1} for the present case.

The evolution of the alongslope current is plotted in Figs. 3b and 4b. Note that $\hat{v}$ in the boundary layer decreased along with the cross-slope velocity. The evolution of the alongslope shear stress, $-\rho_0\nu(\partial\hat{v}/\partial\hat{z})$, is plotted in Figs. 3e and 4e. Although the shear is high above the mixed layer, the stress is negligible there, owing to the small eddy viscosity. Note also that the shear stress at the boundary decreased in time. MacCready and Rhines (1991) find that the along-slope shear stress decreases as the transport decreases, as shown by taking the $\hat{z}$ integral of Eq. (2.3):

$$f\rho_0 \int_0^\infty \hat{u}\,d\hat{z} = -\rho_0\left(\nu\frac{\partial\hat{v}}{\partial\hat{z}}\right)_{\hat{z}=0} - \rho_0\int_0^\infty \frac{\partial\hat{v}}{\partial t}\,d\hat{z} \quad (3.2)$$

and assuming that the acceleration (third term) is small after an early time. Both the transport and the shear stress decreased to small, near-steady values by day 9, yet they remained closely balanced. Thus, either would be useful measures of the ability of the boundary layer to spin down the interior. Although there is persistent time variation of the alongslope velocity profile of Fig. 4b above the mixed layer, its integral is about an order of magnitude smaller than the late-time shear stress at the boundary. One may, in fact, show that the acceleration term is O(S) compared with the first two terms in (3.2), using the theory to be presented in section 4. The acceleration term in (3.2) may also be large owing to inertial oscillations, but in this instance it merely serves to cancel with the oscillations in the transport, leading to an along-slope boundary stress that looks like a smoothed version of the transport.

By day 9 the transport appeared to have achieved a constant, small value. It turns out, however, that it was not truly steady, as one might guess from the continued changes in the alongslope velocity and density profiles. We may integrate the buoyancy equation (2.4) to form an expression for the upslope transport:

$$\int_0^\infty \hat{u}\,d\hat{z} = \frac{1}{\alpha N^2}\int_0^\infty \frac{\partial B}{\partial t}\,d\hat{z} + \frac{\kappa_\infty}{\alpha}. \quad (3.3)$$

The expected steady value, κ_∞/α, is evident here, but is attained only when the buoyancy term in (3.3) becomes vanishingly small. In Fig. 4 the transport by day 18 was about 0.03 m^2 s^{-1}, three times the steady value, $\kappa_\infty/\alpha = 0.01$ m^2 s^{-1}. The difference was due to persistent changes in the buoyancy term of (3.3). This profile continued to change indefinitely; by day 60 of the same integration (not shown) the transport had dropped only to 0.025 m^2 s^{-1}. This is an interesting comment on steady solutions to the problem, indicating that although they must ultimately be correct, they may take an extremely long time to develop in practice. Differences persist because the interior velocity has not yet achieved that of the steady solution. One does not, however, know exactly what that steady velocity will be, since it is a function of the final diffusivity profile (see Garrett 1991).

The diffusivelike thickening of the alongslope velocity boundary layer, seen in Fig. 4b outside of the mixed layer, is a very peculiar feature of flows on a slope with rotation and stratification. MacCready and Rhines (1991) find such a thickening in their integrations with constant diffusivity, and develop an approximate equation to describe the behavior, calling it "slow diffusion." This is addressed for the variable diffusivity case in section 4. The "job" of this diffusive change in the alongslope flow is to bring it to the value required by the steady solution. This will, of course, take infinitely long, as our model fluid is infinitely deep. Nevertheless, the transport does *nearly* achieve its

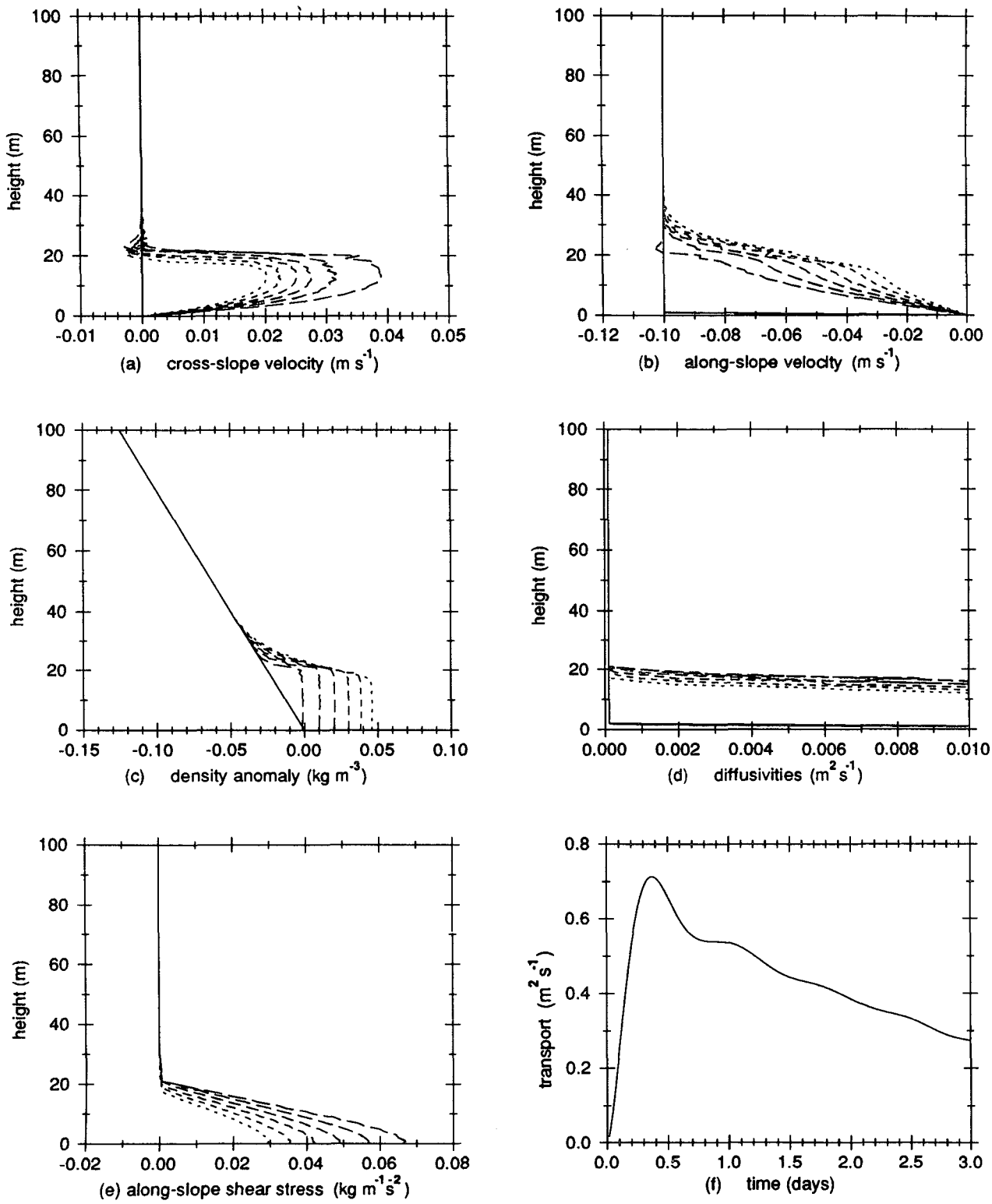

FIG. 3. Output from a three-day numerical integration of (2.2)–(2.4) with: $f = 10^{-4}$ s^{-1}, $N = 3.5 \times 10^{-3}$ s^{-1}, $\alpha = 10^{-2}$, $V = -0.1$ m s^{-1} (upwelling favorable). Plotted are (a) upslope velocity $\hat{u}$, (b) alongslope velocity $\hat{v}$, (c) density perturbation $\rho - \rho_0$, (d) eddy diffusivity coefficients ν and κ, (e) alongslope shear stress $-\rho_0 \nu(\partial \hat{v}/\partial \hat{z})$, all versus $\hat{z}$, and (f) cross-slope transport versus time. Plots (a)–(e) show the profile of the quantity in question at seven different times during the integration: day 0 (solid line), day 0.5 (dashed line with longest dashes), and so on, every half day, until day 3 (dashed line with shortest dashes). Initially the transport was about 0.7 m^2 s^{-1}, as we might expect from steady Ekman theory.

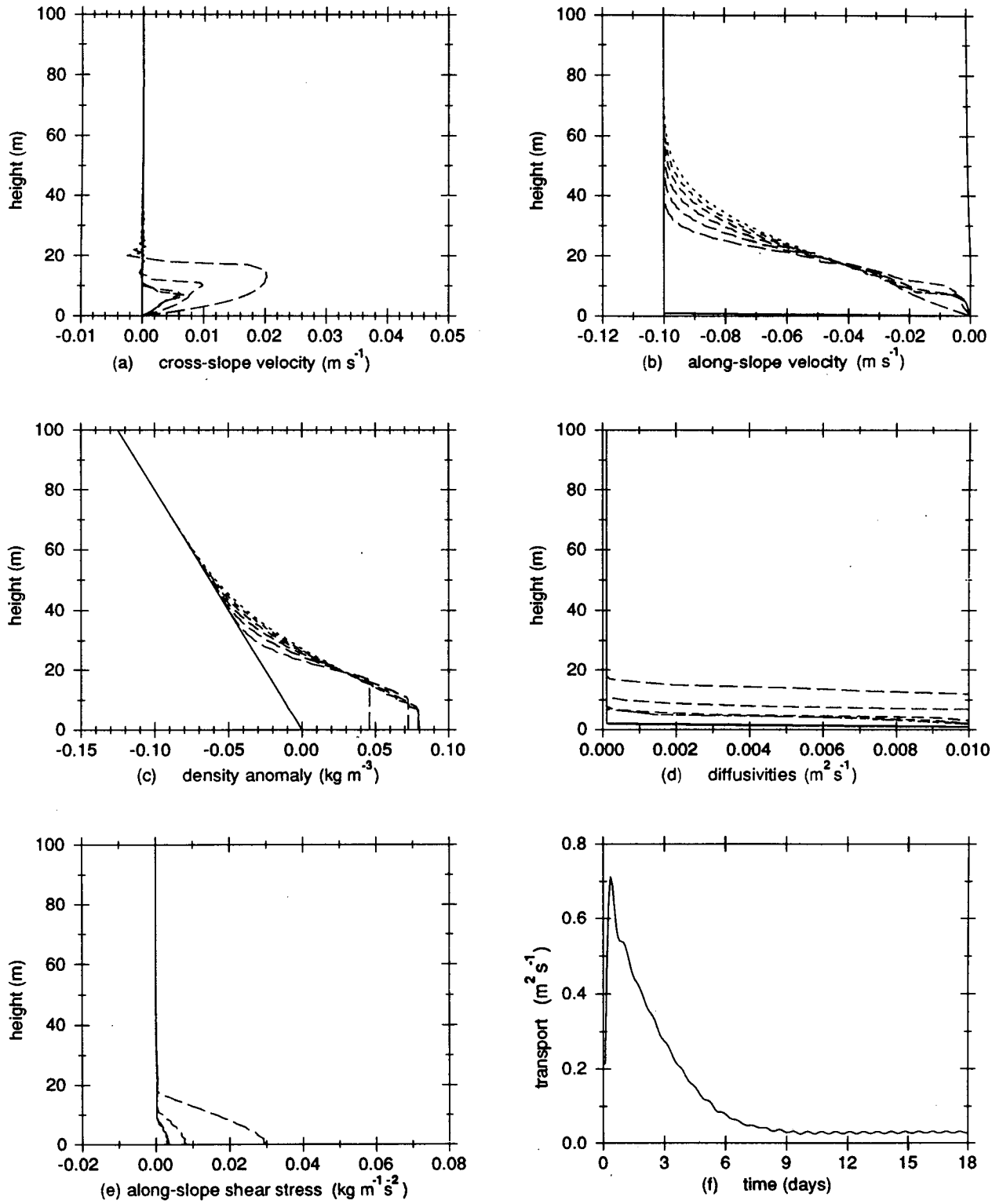

FIG. 4. Same integration as in Fig. 3 but carried out to 18 days. The curves in (a)–(e) are plotted every three days in this case, day 0 (solid line), day 3 (dashed line with longest dashes), and so on, to day 18 (dashed line with shortest dashes). By day 9 the transport had fallen to near zero, and the boundary layer was almost steady, except for the diffusivelike thickening of the $\rho-\rho_0$ and $\hat{v}$ profiles outside of the mixed layer.

steady value over the relatively short shutdown time, indicating that the steady solutions may be more applicable for their predictions of the transport than for their predictions of the interior velocity. Although the early shutdown of the transport is not particularly sensitive to ν_∞ or κ_∞, the slow diffusion process is very much affected by the values of these diffusivities, of which we have only a vague idea in the real ocean.

The evolution of the density anomaly, $\rho - \rho_0$, is plotted in Figs. 3c and 4c. The density was nearly constant in depth within the mixed layer, as we assumed in our approximate solution in the previous section, and the value of the density within the mixed layer increased over time, as the stratification was advected upslope by the $\hat{u}$-velocity field. (The density is actually plotted versus z, the true vertical coordinate, and is then mapped into $\hat{z}$ to make the plot. This is done so that one may judge easily if a given profile is statically stable: a vertical line in the density profile is neutrally stable.) Note that the density anomaly showed the same diffusive thickening as the alongslope velocity. The alongslope flow was almost exactly in thermal-wind balance with the density field in the region beyond the mixed layer.

The diffusivities, shown in Figs. 3d and 4d, show that the flow initially formed a turbulent boundary layer about 20 m thick. Interestingly, the mixed-layer height *decreased* in time, eventually settling at about 8 m. The reason was presumably a combination of decreasing alongslope shear in the mixed layer, as well as some small restratification. This process, which cannot be reproduced by standard slab models, seems to be peculiar to sloping boundaries (no such thinning was observed in numerical integrations with $\alpha = 0$) and is certainly connected with the decreased bottom shear stress associated with shutdown.

b. *Downwelling favorable case*

Figures 5 and 6 present the evolution of the boundary layer for the case where $V = +0.1$ m s^{-1} (downwelling favorable). This is the same sense as the flow in the Deep Western Boundary Current in the North Atlantic. All other parameters were as in Figs. 3 and 4. As before, Fig. 5 is a three-day integration, and Fig. 6 is the same run taken out to 18 days.

The main difference between this run and the upwelling-favorable run was that here the turbulent mixed layer continued to grow in height throughout the integration. The reason was that the downslope flow tended to push lighter water under heavier, leading to convective instability (or, as our model sees it, a low Ri due to low values of $\partial\rho/\partial\hat{z}$, and hence high diffusivities). This asymmetry in mixed-layer height during upwelling versus downwelling-favorable flows has been observed previously in numerical experiments and in ocean flows by both Weatherly and Martin (1978) and Trowbridge and Lentz (1991).

Initially the cross-slope flow, $\hat{u}$, looked Ekman-like, as in the early section of Fig. 3a. Later it thickened, and decreased in magnitude. The transport history, Figs. 5f and 6f, shows that the integral of the cross-slope velocity decreased in magnitude as well, although not as quickly as in the upwelling-favorable case, and had clearly not completely shut down by day 18. The theory presented in section 2 implies that the difference in the transport decay was mainly due to the different mixed-layer heights in the two cases. Recall that we found that the decay time scale increased linearly with H in (2.19). The alongslope stress at the boundary, which, as we have said, should be linked with the transport, also decreased in time (Figs. 5e and 6e).

At the end of the integration the cross-slope flow, Fig. 6a, formed a weak double jet with slight upslope flow near the boundary and downslope flow near the top of the mixed layer. The upwelling part was the first sign of the steady solution that always has an upslope transport κ_∞/α. Garrett (1990) relates the double jet to boundary mixing, showing that it advectively restratifies the fluid by slumping of the vertical isopycnals, while diffusion is trying to remove any stratification that arises in the mixed layer.

The alongslope velocity, plotted in Figs. 5b and 6b, tended toward a simple linear shear over time, going from zero to V over the thickness of the mixed layer, and the predicted thickness, $H_{\min}$, is 81.6 m, very close to the value we see by day 18 in Fig. 6c. The alongslope flow was very close to thermal wind balance over all of the boundary layer, unlike the upwelling-favorable case where diffusive effects remained important within the mixed layer.

The diffusivities, Figs. 5d and 6d, were initially high in the mixed layer, but dropped off gradually at later time, owing to the slowly decreasing velocity shear, as well as a finite stratification within the mixed layer itself at later time, consistent with Garret's (1991) prediction of the final Richardson number.

c. *Comparison of theoretical and numerical results*

From the full numerical solutions we may check the accuracy of our analytic shutdown time prediction, $D\tau_0$. Figures 7 and 8 show the cross-slope transport versus time for six different full numerical solutions (two of which were shown before in detail). We plot the (absolute value of) transport on a log scale versus a linear time scale. Exponential decay, which (2.19) predicts for constant H, shows up as a straight line on such a plot. Figure 7 is for three upwelling-favorable runs, all with $V = -0.1$ m s^{-1}, with three different slope angles, $\alpha = 0.02$, 0.01, and 0.005. The upwelling favorable cases all had relatively constant mixed-layer thicknesses, so we expect nearly exponential decay, which is borne out by the linearity of the curves during the shutdown. Figure 8 is for three downwelling favorable runs, again with $\alpha = 0.02$, 0.01, and 0.005,

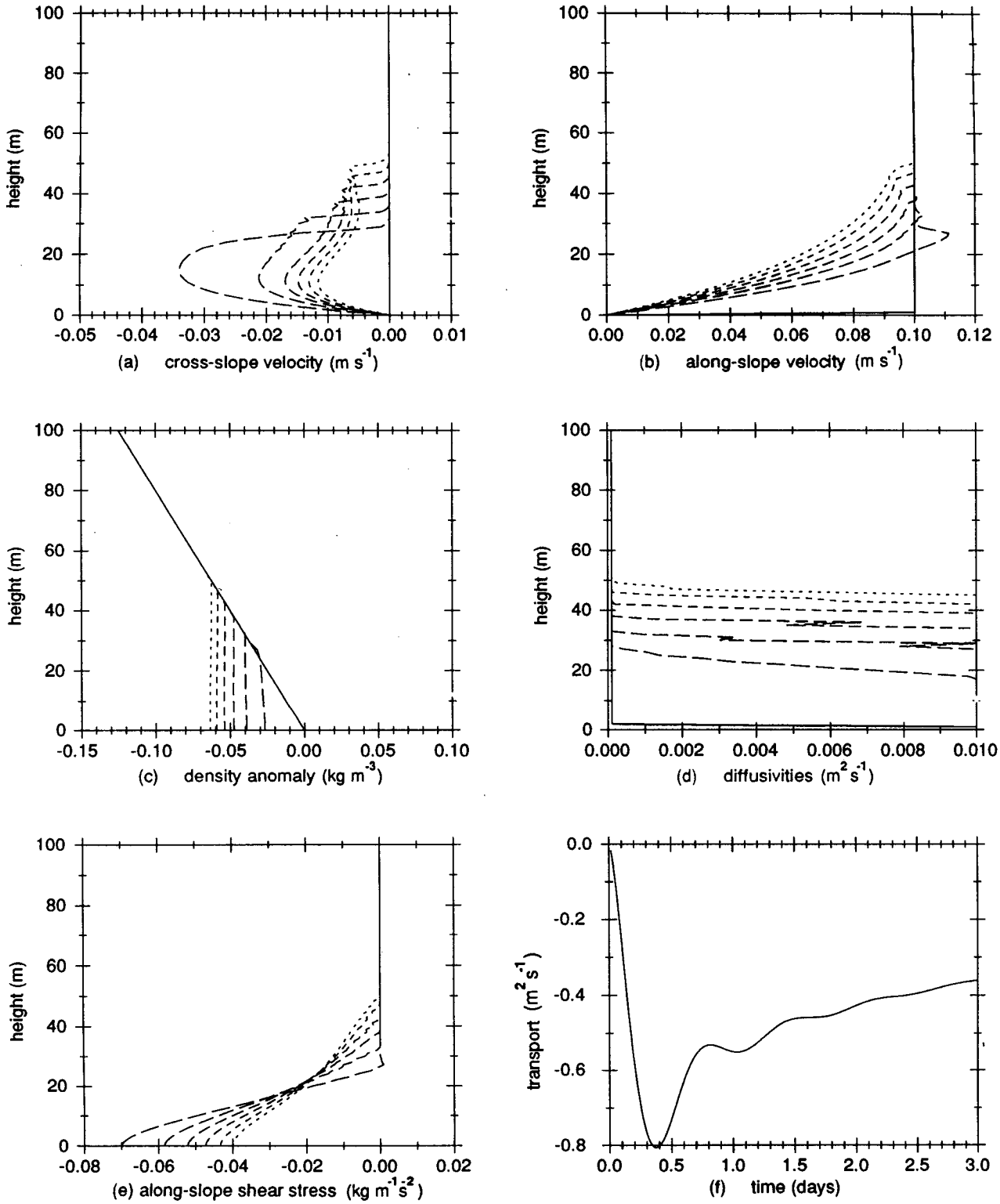

FIG. 5. Output from a three-day numerical integration of (2.2)–(2.4), parameters as in Fig. 3 except $V = +0.1$ m s^{-1} (downwelling favorable). Plotted are (a) upslope velocity $\hat{u}$, (b) alongslope velocity $\hat{v}$, (c) density perturbation $\rho - \rho_0$, (d) eddy diffusivity coefficients ν and κ, (e) alongslope shear stress $-\rho_0 \nu(\partial \hat{v}/\partial \hat{z})$, all versus $\hat{z}$, and (f) cross-slope transport versus time. Plots (a)–(e) show the profile of the quantity in question at seven different times during the integration: day 0 (solid line), day 0.5 (dashed line with longest dashes), and so on, every half day, until day 3 (dashed line with shortest dashes). The cross-slope transport tends to push lighter water down under heavier, leading to an unstable density profile and hence a progressively thicker mixed layer.

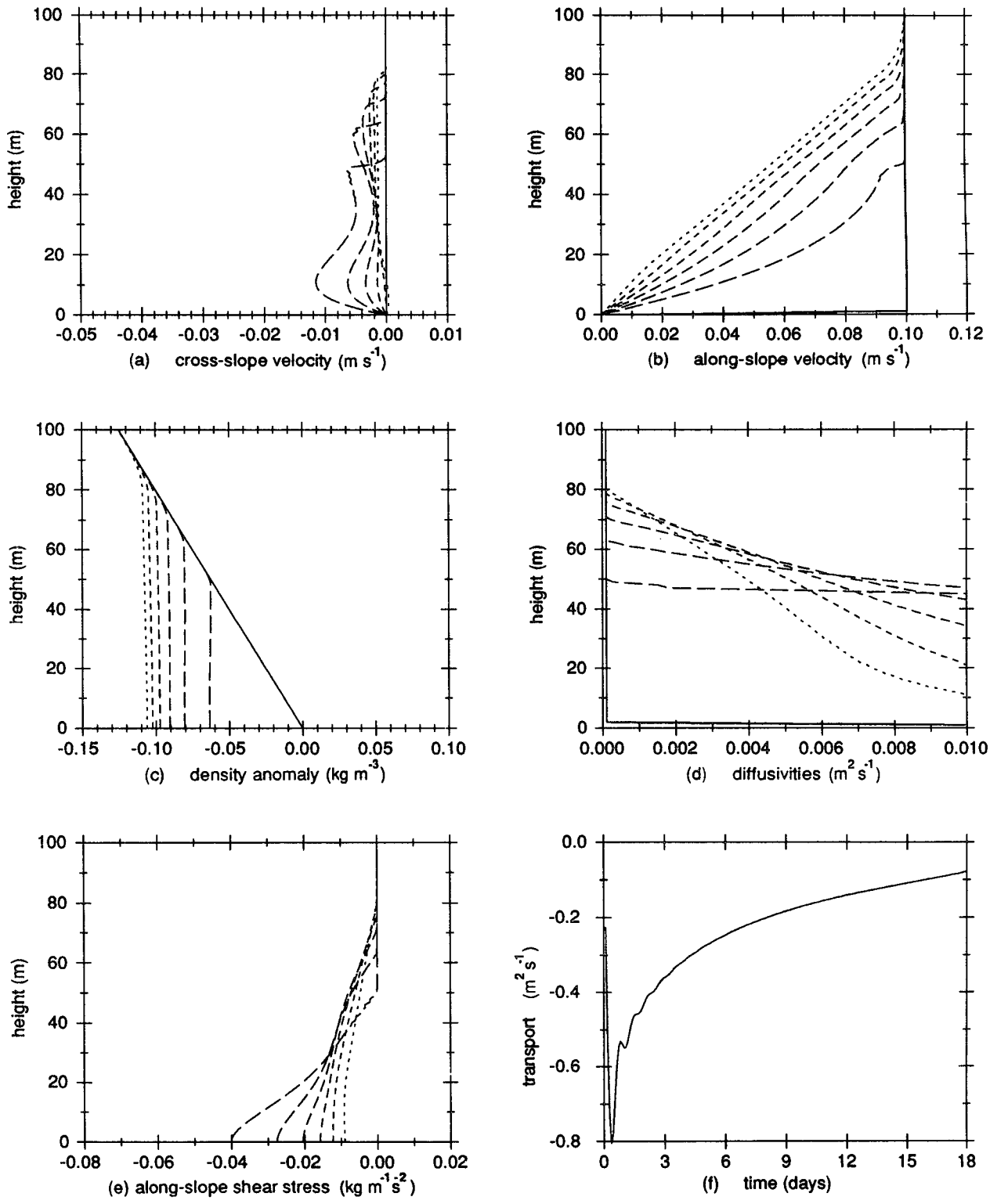

FIG. 6. Same integration as Fig. 5 but carried out to 18 days. The curves in (a)–(e) are plotted every three days in this case, day 0 (solid line), day 3 (dashed line with longest dashes), and so on, to day 18 (dashed line with shortest dashes). Again the magnitude of the transport (f) decreases with time, although not as rapidly as in Fig. 4f, owing to the greater mixed-layer thickness. The alongslope flow (b) gradually assumes a linear shear from zero to V over the mixed layer.

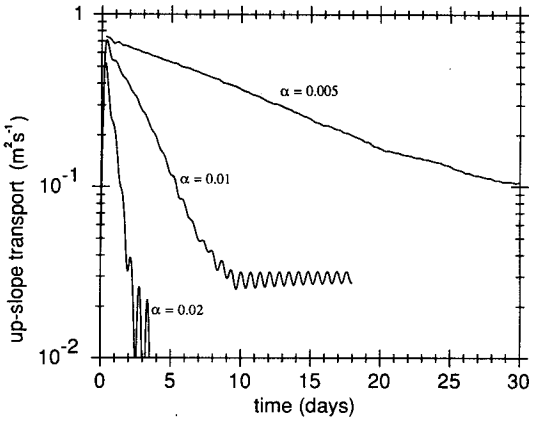

FIG. 7. Upslope transport (log scale) versus time for three numerical runs. All parameters were as in Fig. 4 (upwelling favorable) except the slope angle, α, which was varied as shown. The transport curves were nearly linear during the initial shutdown, indicating that the decay was close to exponential, as in (2.19). The strong dependence of the shutdown time, $Df/(N\alpha)^2$, on α is evident in these curves.

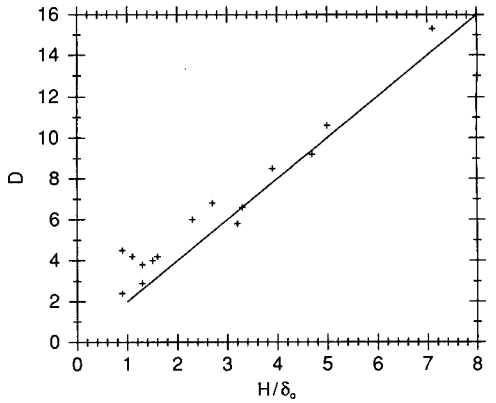

FIG. 9. Value of the factor D (solid line) from (2.20), versus H/δ_0, the ratio of the mixed-layer thickness to the nominal Ekman layer thickness, $(\nu_0/\Omega)^{1/2}$. Equation (2.19) predicts that, for constant H, the cross-slope transport will decay exponentially in a time scale $Df/(N\alpha)^2$. Also plotted (+) are values of D from (3.4), figured at various times during the six numerical solutions to the full equations shown in Figs. 7 and 8. Although H varied during a given run, especially for the downwelling-favorable cases, we may still calculate a value of D at a given time. These observed values of D from the numerical runs compare well with the analytic predictions.

and $V = +0.1$ m s^{-1}. The curves are less linear than in Fig. 7, and in particular the slope decreased in magnitude at later times when the boundary-layer thickness was greater. This is consistent with the longer shutdown time scale we predict for greater H.

We may compare our analytic theory and the full numerical solutions at any time during a numerical run, and this is done in Fig. 9. The solid line in this figure is the factor D, which multiplies τ_0 to give the shutdown time from the theory, plotted versus H/δ_0. Thus, D has a slope of 2 in this graph. The solution curve stops for $H/\delta_0 < 1$, since our solution is for $H \gg \delta_0$, but only diverges markedly from the full solution when $H/\delta_0 < 1$ (MacCready 1991).

The crosses (+) in Fig. 9 are values of D observed in the six full numerical solutions of Figs. 7 and 8.

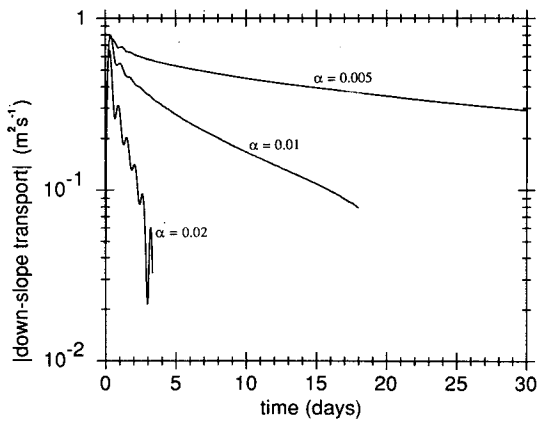

FIG. 8. Absolute value of the downslope transport (log scale) versus time for three numerical runs. All parameters were as in Fig. 6 (downwelling favorable) except the slope angle, α, which was varied as shown. The transport decreased more slowly for these cases than those in Fig. 7, owing to the greater mixed-layer thickness.

Although H was changing with time in these runs, we may estimate a value of D *at a given time* by solving (2.19) for D, giving

$$D = -M\left(\tau_0 \frac{\partial M}{\partial t}\right)^{-1}. \qquad (3.4)$$

All the terms on the right-hand side of (3.4) are either known or are easily found from the transport plots. Then, by noting the mixed-layer thickness at that time (defined as the height where $\nu \to \nu_\infty$), we arrive at a point to plot on Fig. 9. For downwelling favorable cases, both the observed D and H changed over time. For any given run points were taken at several different times, starting when $t = 1$ day, and going to the time when the transport had approximately e-folded. As one can see in Fig. 9, the agreement between the theory and the full numerical solutions is fairly good, even over a wide range of boundary-layer thicknesses, lending credence to our analytic estimate of the shutdown time.

4. Long-time evolution; the slow-diffusion equation

As the cross-slope transport decays, the flow described in the previous sections continues to adjust, with gradual penetration of the momentum profile upward above the mixed layer (Figs. 4b, c, and marginally in 6b, c), drawing the interior along-slope velocity toward that of Thorpe's steady solution (MacCready and Rhines 1991). The one-dimensional system seeks in this way to establish a steady flow obeying the global connection between cross-slope transport and interior density diffusion, the steady limit of (3.3).

What makes the effect so striking is that the classic Ekman layer never diffuses beyond a distance δ_0 from the boundary. The reason for the continued diffusivelike thickening of the alongslope velocity profile can be seen from the following argument involving the meridional (i.e., $\hat{x}$, $\hat{z}$) circulation: first, any vertical divergence of along-slope shear stress (e.g., curvature in the velocity field) will have some cross-slope transport associated with it (by 2.3); second, that motion advects buoyancy, B, across the slope; and third, the displacement of isopycnal surfaces will quickly require, via the thermal wind, a decrease in magnitude of the alongslope current, thus providing a pseudo diffusion of momentum normal to the bottom. Similar diffusivelike thickening is seen by Gill (1981) and Garrett (1982) in the context of a sloping shear region in the ocean interior, with constant coefficients of diffusivity. We call this thickening of the alongslope boundary layer slow diffusion: diffusion because it obeys a diffusion equation, and slow because it happens (for $\sigma > 1$) at a slower rate than would be the case for a simple nonrotating boundary layer with the same viscosity.

To develop the equation describing slow diffusion, we assume in MacCready and Rhines (1991) that the along-slope flow is in thermal wind balance. This approximation, which amounts to having a small Rossby number and a small Ekman number in the cross-slope momentum equation, (2.2), is suggested by scaling of the equations, and by examination of numerical integrations. While the approximations cannot hold very close to the boundary, they become increasingly accurate at larger distance. Here we want to incorporate nonuniform, time-dependent diffusivities in the theory, appropriate to our numerical experiments. First, ignore the acceleration and diffusive terms in the cross-slope momentum balance, leaving:

$$f(\hat{v} - V) = \alpha B. \tag{4.1}$$

Take derivatives of this to form:

$$\frac{\partial B}{\partial t} = \frac{f}{\alpha}\frac{\partial \hat{v}}{\partial t}, \quad \frac{\partial B}{\partial \hat{z}} = \frac{f}{\alpha}\frac{\partial \hat{v}}{\partial \hat{z}}. \tag{4.2}$$

These are substituted into the buoyancy equation, (2.4), which may then be written as

$$f\hat{u} = \frac{1}{S}\frac{\partial \hat{v}}{\partial t} + \frac{f}{\sigma\alpha}\frac{\partial \nu}{\partial \hat{z}} - \frac{1}{S\sigma}\frac{\partial}{\partial \hat{z}}\left(\nu\frac{\partial \hat{v}}{\partial \hat{z}}\right). \tag{4.3}$$

This is substituted into the alongslope momentum equation, (2.3), and the result rearranged to find

$$\boxed{\frac{\partial \hat{v}}{\partial t} = \frac{-f}{\sigma\alpha}\left(\frac{S}{1+S}\right)\frac{\partial \nu}{\partial \hat{z}} + \left(\frac{1/\sigma + S}{1+S}\right)\frac{\partial}{\partial \hat{z}}\left(\nu\frac{\partial \hat{v}}{\partial \hat{z}}\right),} \tag{4.4}$$

which is the slow diffusion equation for nonuniform, time-dependent coefficients. When the diffusivity is constant the second term drops out, and the expression reduces to the laminar slow diffusion equation of MacCready and Rhines (1991). Equation (4.4) tells us that in regions where the alongslope flow is in thermal wind balance and the diffusivities constant, the alongslope momentum profile will develop as in a diffusive process, tending to thicken indefinitely. Yet both ν and κ are involved in this development, through the implicit role of the buoyancy of the fluid.

To compare the slow diffusion equation with the full solution, numerical integrations of (4.4) were carried out (Figs. 10 and 11) with the values of the diffusivities taken from the exact numerical model runs. They give a good representation of the evolution of $\hat{v}(\hat{z}, t)$ for later times, except within the mixed layer for the upwelling favorable case. There the viscous effects are not negligible [recall that our derivation of (4.4) required a small Ekman number in the cross-slope momentum equation].

For the upwelling favorable case, outside of the mixed layer, the second term in (4.4) is unimportant and the alongslope boundary layer thickens like

$$\left(\frac{1/\sigma + S}{1+S}\right)^{1/2}(\nu t)^{1/2}. \tag{4.5}$$

Note that when $\sigma = 1$, as in our numerical integrations, (4.5) reduces to $(\nu t)^{1/2}$, as in a normal diffusion equation, while for $\sigma > 1$, as is typical of molecular diffusion or situations where internal waves may carry momentum, the diffusion may be much slower.

In the downwelling-favorable case the slow diffusion equation (Fig. 11) predicts well the nearly linear variation of $\hat{v}$ with depth seen in Fig. 6b, which Trowbridge and Lentz suggest as a possible steady solution (see 2.24). Garrett (1991) gives an important insight into the slow diffusion equation that connects it with this linear shear prediction. He suggests that at later times, that is, $t \gg D\tau_0$, the acceleration term in (4.4) may become negligible. Dropping this term and integrating the equation from $\hat{z}$ to ∞ he finds

$$\frac{\partial \hat{v}}{\partial \hat{z}} = \frac{f}{\alpha}\left(\frac{S}{1+\sigma S}\right)(1 - \nu_\infty/\nu). \tag{4.6}$$

This predicts, as we would hope, zero shear in the exterior where $\nu = \nu_\infty$, and in the mixed layer it predicts a shear of $(f/\alpha)[S/(1+\sigma S)]$, provided $\nu \gg \nu_\infty$. The shear predicted in section 2 is $V/H_{\min}$, which is equal to $N^2\alpha/f$, or $(f/\alpha)S$. Hence, (4.6) represents a modification to the prediction from section 2, decreasing the shear in the boundary layer by a factor $(1+\sigma S)^{-1}$.

Since the stratification is assumed to be in thermal wind balance with the alongslope flow, Garrett is also able to predict the final Richardson number of the flow, and hence its final diffusivity. These predictions are, however, sensitive to the Ridependence of mixing that is assumed. If the region of higher diffusivities extends to larger Ri (say 0.5 or greater) then Garrett's prediction

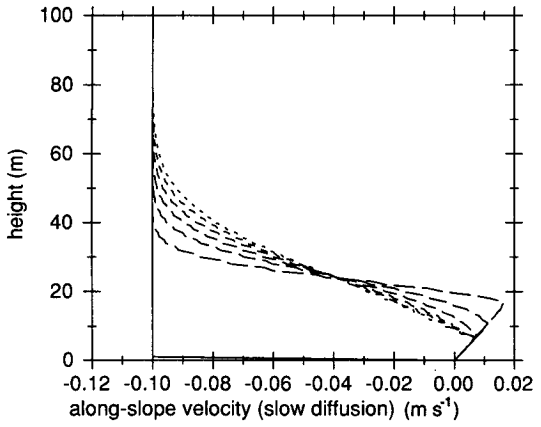

FIG. 10. Numerical solution to the slow diffusion equation (4.4) for the 18-day integration shown in Fig. 4 (upwelling favorable). As in Fig. 4b, the seven different profiles are the along-slope velocity at seven different times in the integration: day 0 (solid line), day 3 (dashed line with longest dashes), and so on, every three days, until day 18 (dashed line with shortest dashes). The slow diffusion equation captures well the diffusivelike thickening of the boundary layer beyond the mixed layer; however, it is clearly wrong in the mixed layer, owing to strong diffusive effects there.

works well, yet with our current choice (Fig. 2) the diffusivity becomes small in the mixed layer at large time, approaching its lower limiting value (the beginning of this fall in the diffusivities is apparent in Fig. 6d). Then the slow diffusion equation remains essentially time dependent and (4.6) is not applicable.

It seems paradoxical that we have a slow diffusion prediction for the upwelling-favorable case that looks like a diffusive penetration of momentum upward from the boundary, yet on the other hand we have established that the boundary shear stress is almost exactly balanced by the Coriolis force on the diminishing cross-slope transport. The resolution is that the slow diffusion solutions are driven by the small shear stress at the top of the boundary layer, seeing that as an apparent boundary stress, while inside the mixed layer such solutions are inaccurate owing to the importance of diffusive effects there.

5. Conclusions

Several recent papers—Weatherly and Martin (1978), Thorpe (1987), Garrett (1990, 1991), MacCready and Rhines (1991), Trowbridge and Lentz (1991), MacCready (1991), and the present work—have begun to illuminate the murky topic of stratified oceanic bottom boundary layers over sloping topography. The authors' interests range from steady to time-dependent solutions, and from momentum dynamics to the mixing of density within the boundary layer. This paper approaches the problem from the point of view of the boundary stress that will slow down bottom currents in the ocean, such as deep western boundary currents. We find that evolving buoyancy forces cause the boundary stress (and its associated Ekman transport) to drop off quasi-exponentially in time, with the fundamental time scale given by $f/(N\alpha)^2$. Thicker mixed layers may have substantially slower decay of their boundary stress than thinner ones. Above the mixed layer the current is slowed in a diffusivelike manner, eventually bringing the interior flow in line with that required by the steady solution.

Our discussion of long-time behavior here and in MacCready and Rhines (1991) is carried out within the one-dimensional framework of the model. The slowness of this process merits examination, however. The three-dimensional ocean is driven primarily by temperature, fresh water, and momentum exchange with the atmosphere above. These forcing effects are transmitted to the deep interior by pressure forces and direct advection. Until we have an appreciation for the rates of invasion of these properties from both sea surface and the benthic boundary layer, we cannot say whether the seafloor drives significant interior circulation or not. The one-dimensional problem by itself suggests the importance of self-propelled circulations driven by boundary mixing, but these may be lost in the face of the other sources of motion and buoyancy.

Although the steady solutions may be achieved only slowly, if ever, it appears that the near-zero boundary stress may evolve much more rapidly (assuming a short shutdown time), and hence be a more robust result. The implications of a low-stress boundary could be considerable. By eliminating fast classical spinup for much of the ocean we have to look for other ways to achieve a global balance of angular momentum. The need for direct measurement of boundary shear stress

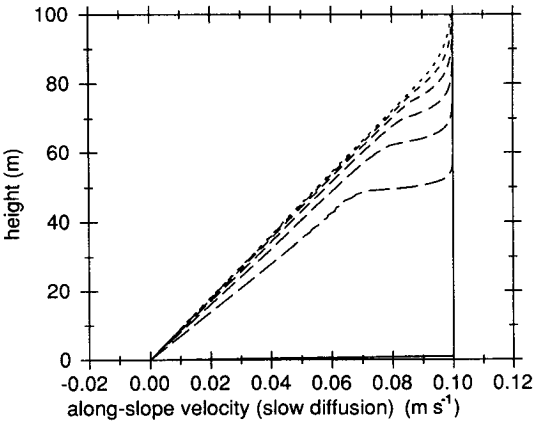

FIG. 11. Numerical solution to the slow diffusion equation (4.4) for the 18-day integration shown in Fig. 6 (downwelling favorable). As in Fig. 6b the seven different profiles are the along-slope velocity at seven different times in the integration: day 0 (solid line), day 3 (dashed line with longest dashes), and so on, every three days, until day 18 (dashed line with shortest dashes). By day 15 (about 1.5 times the shutdown time) the slow diffusion solution gives a good representation of the along-slope flow. The linear shear is very similar in form and thickness (H_{min} = 81.6 m) to that proposed by Trowbridge and Lentz (1991) and discussed in section 2d.

is clear. Evaluation of inviscid form drag on deep-sea topography (both at the small scale of internal waves and the great scale of planetary waves) becomes particularly important (though it must be realized that energy has to dissipated in a statistically steady ocean driven by winds; inviscid momentum drag must be accompanied by small-scale turbulent energy dissipation, whether it occurs in the boundary layer or in the interior).

Full two- and three-dimensional problems (like the laboratory experiments in MacCready and Rhines 1991) should now be pursued. Preliminary laboratory studies of flow in a basin with both flat plains and elevated ridges suggest that the slipperiness of flow over slopes is indeed important, and may set the stage for strong instability between the jets that run along ridges and the spundown fluid overlying the adjacent abyssal plain.

There are many different questions one might ask of models of deep-ocean boundary layers. Here we have shown the development of momentum, boundary-layer transport, and buoyancy fields for an assumed model of Richardson number–dependent mixing coefficients. While sensitivity to the form of this dependence did not seem too great, the evolving profiles of ν and κ in the mixed layer are themselves quite sensitive. Thus, if one is interested in flux of a benthic tracer (radon, biological communities, sediment, etc.) through the mixed layer, further exploration of the mixing laws should be made. Indeed, it might be that the nephelometer and trace chemistry observations could constrain $\nu(\mathrm{Ri})$ and $\kappa(\mathrm{Ri})$ within the context of this model.

While we have not applied these ideas in detail to observed deep-ocean flows, we are particularly interested in the rapid deep western boundary currents of the World Ocean. These key elements of the global circulation often begin as gravity currents, for instance, where flows spill over the sill in the Denmark Strait. Barringer and Price (1990) suggest that a simple balance between the buoyancy, bottom drag, and entrainment drag determines how deep these water masses fall before leveling out and flowing quasi-horizontally along the sloping boundary (so that improved models of bottom stress are of great interest). If it were true that Ekman flux were carrying fluid across slope (often downslope) at the classically predicted rate, then the water within these currents would be recycled through the boundary layer or otherwise bled off into the interior remarkably quickly; yet it does not appear to happen. Nor does the momentum drag on the deep boundary currents appear to be as great as Ekman theory would predict; essentially the classic spindown time of a 500-m thick boundary current with a 50-m thick benthic mixed layer is about 10 days! While global pressure gradients are available to continually drive boundary currents after they have gravitationally fallen down from their source regions, the level of frictional damping would alter the apparent long-distance integrity of these boundary currents [one may see the role of diffusion in Kawase's (1987) model of source-driven deep circulation]. In addition, the classic calculation of spindown of such a current would also involve production of remarkable counterflows reaching to the top of the ocean, for these currents tend to have a width at least as great as the gravest internal Rossby deformation radius.

It is not simple, though, to apply shutdown theory to actual deep flows in the ocean. The theory was developed for an idealized situation, with flat isopycnals intersecting the slope. The crucial quantity allowing shutdown, however, is not just the ambient buoyancy frequency in the fluid, but the existence of a gradient of density on the slope itself, allowing the cross-slope transport to change the density structure. In some boundary currents driven by overflows of heavy water the density structure may be far from our idealized situation, with constant density on the slope across the entire width of the current. In this case shutdown theory would not be applicable. What then of the actual dynamics of the Deep Western Boundary Current in the North Atlantic?

A final puzzle for future observational and theoretical work lies in our inability to separate the upstream *preconditioning* of the flow (which may tend to insulate the current from the slope by a cushion of water already in thermal-wind balance, as in the Straits of Florida), from the shutdown or spindown processes, all of which eventually leave the interior flow relatively free from frictional effects at the boundary.

Acknowledgments. This work was supported by Office of Naval Research Grant N00014-86-K-0690, and National Science Foundation Grant 89-16009. The authors wish to thank Chris Garrett and John Trowbridge for many enjoyable discussions.

REFERENCES

Armi, L., and R. C. Millard, 1976: The bottom boundary layer of the deep ocean. *J. Geophys. Res.*, **81**, 4983–4990.

Barringer, M. O., and J. F. Price, 1990: A simple model of the descending Mediterranean outflow plume. *The Physical Oceanography of Sea Straits*, L. J. Pratt, Ed. Kluwer Academic, 537–544.

Dewey, R. K., P. H. LeBlond, and W. R. Crawford, 1988: The turbulent bottom boundary layer and its influence on local dynamics over the continental shelf. *Dyn. Atmos. Oceans*, **12**, 143–172.

Ezer, T., and G. L. Weatherly, 1990: A numerical study of the interaction between a deep cold jet and the bottom boundary layer of the ocean. *J. Phys. Oceanogr.*, **20**, 801–816.

Garrett, C., 1982: On spindown in the ocean interior. *J. Phys. Oceanogr.*, **12**, 989–993.

——, 1990: The role of secondary circulation in boundary mixing. *J. Geophys. Res.*, **95**, 3181–3188.

——, 1991: Marginal mixing theories. *Atmos.-Ocean*, **29**, 313–339.

Gill, A. E., 1981: Homogeneous intrusions in a rotating stratified fluid. *J. Fluid Mech.*, **103**, 275–295.

Greenspan, H. P., 1969: *The Theory of Rotating Fluids*. Cambridge University Press, 328 pp.

Gregg, M. C., 1987: Diapycnal mixing in the thermocline: A review. *J. Geophys. Res.*, **92,** 5249–5286.

Holton, J. R., 1965: The influence of viscous boundary layers on transient motions in a stratified rotating fluid: Part I. *J. Atmos. Sci.*, **22,** 402–411.

——, 1967: The diurnal boundary layer wind oscillation above sloping terrain. *Tellus,* **19,** 199–205.

Hsueh, Y., 1969: Buoyant Ekman layer. *Phys. Fluids,* **12,** 1757–1762.

Kawase, M., 1987: Establishment of deep ocean circulation driven by deep-water production. *J. Phys. Oceanogr.*, **17,** 2294–2317.

Lentz, S. J., and J. H. Trowbridge, 1991: The bottom boundary layer over the northern California shelf. *J. Phys. Oceanogr.*, **21,** 1186–1201.

MacCready, P., 1991: Frictional slowing of rotating, stratified flow over a sloping boundary. Ph.D. thesis, University of Washington, 131 pp.

——, and P. B. Rhines, 1991: Buoyant inhibition of Ekman transport on a slope and its effect on stratified spin-up. *J. Fluid Mech.*, **223,** 631–661.

Mellor, G. L., and T. Yamada, 1974: A hierarchy of turbulence closure models for planetary boundary layers. *J. Atmos. Sci.*, **31,** 1791–1806.

Munk, W. H., 1966: Abyssal recipes. *Deep-Sea Res.*, **13,** 707–730.

Pedlosky, J., 1987: *Geophysical Fluid Dynamics.* Springer-Verlag, 710 pp.

Phillips, O. M., 1970: On flows induced by diffusion in a stably stratified fluid. *Deep-Sea Res.*, **17,** 435–443.

Pollard, R. T., P. B. Rhines, and R. O. R. Y. Thompson, 1973: The deepening of the wind-mixed layer. *Geophys. Fluid Dyn.*, **3,** 381–404.

Price, J. F., R. A. Weller, and R. Pinkel, 1986: Diurnal Cycling: Observations and models of the upper-ocean response to diurnal heating, cooling, and wind mixing. *J. Geophys. Res.*, **91,** 8411–8427.

Rhines, P. B., and P. MacCready, 1989: Boundary control over the large-scale circulation. *Proc. Fifth 'Aha Huliko'a Hawiian Winter Workshop on Parameterization of Small-Scale Processes,* Hawaii Institute of Geophysics, Honolulu, 75–97.

Thorpe, S. A., 1987: Current and temperature variability on the continental slope. *Phil. Trans. Roy. Soc. Lond.*, **A323,** 471–517.

Trowbridge, J. H., and S. J. Lentz, 1991: Asymmetric Behavior of an oceanic boundary layer above a sloping bottom. *J. Phys. Oceanogr.*, **21,** 1171–1185.

Trump, C. L., 1983: A current-induced Ekman spiral in the St. Lawrence estuary. *J. Phys. Oceanogr.*, **13,** 1540–1543.

Walin, G., 1969: Some aspects of time-dependent motion of a stratified rotating fluid. *J. Fluid Mech.*, **36,** 289–307.

Weatherly, G. L., and P. J. Martin, 1978: On the structure and dynamics of the oceanic bottom boundary layer. *J. Phys. Oceanogr.*, **8,** 557–570.